

## **X-ray Photoelectron Spectroscopic and Raman microscopic investigation of the variscite group minerals: Variscite, strengite, scorodite and mansfieldite**

— [Source link](#) 

J. Theo Kloprogge, J. Theo Kloprogge, Barry J. Wood





**Institutions:** University of Queensland, University of the Philippines Visayas

**Published on:** 05 Oct 2017 - Spectrochimica Acta Part A: Molecular and Biomolecular Spectroscopy (Elsevier)

**Topics:** Strengite, Scorodite and Raman spectroscopy

Related papers:

- [Raman Microscopy Study of Tyrolite: A Multi-Anion Arsenate Mineral](#)
- [Raman Spectroscopic Study of Vivianites of Different Origins](#)
- [A vibrational spectroscopic study of the phosphate mineral cyrilovite  \$\text{Na}\(\text{Fe}^{3+}\)\_3\(\text{PO}\_4\)\_2\(\text{OH}\)\_4 \cdot 2\(\text{H}\_2\text{O}\)\$  and in comparison with wardite.](#)
- [Vibrational spectroscopic study of the minerals cavansite and pentagonite  \$\text{Ca}\(\text{V}\_4\text{O}\)\text{Si}\_4\text{O}\_{10} \cdot 4\text{H}\_2\text{O}\$](#)
- [Raman and infrared spectroscopy of the manganese arsenate mineral allactite.](#)

Share this paper:    

View more about this paper here: <https://typeset.io/papers/x-ray-photoelectron-spectroscopic-and-raman-microscopic-2hkagi7rvd>

## Accepted Manuscript

X-ray Photoelectron Spectroscopic and Raman microscopic investigation of the variscite group minerals: Variscite, strengite, scorodite and mansfieldite

J. Theo Kloprogge, Barry J. Wood



PII: S1386-1425(17)30418-3  
DOI: doi: [10.1016/j.saa.2017.05.042](https://doi.org/10.1016/j.saa.2017.05.042)  
Reference: SAA 15184

To appear in: *Spectrochimica Acta Part A: Molecular and Biomolecular Spectroscopy*

Received date: 16 March 2017  
Revised date: 27 April 2017  
Accepted date: 19 May 2017

Please cite this article as: J. Theo Kloprogge, Barry J. Wood , X-ray Photoelectron Spectroscopic and Raman microscopic investigation of the variscite group minerals: Variscite, strengite, scorodite and mansfieldite, *Spectrochimica Acta Part A: Molecular and Biomolecular Spectroscopy* (2017), doi: [10.1016/j.saa.2017.05.042](https://doi.org/10.1016/j.saa.2017.05.042)

This is a PDF file of an unedited manuscript that has been accepted for publication. As a service to our customers we are providing this early version of the manuscript. The manuscript will undergo copyediting, typesetting, and review of the resulting proof before it is published in its final form. Please note that during the production process errors may be discovered which could affect the content, and all legal disclaimers that apply to the journal pertain.

**X-ray Photoelectron Spectroscopic and Raman  
microscopic investigation of the variscite group minerals:  
variscite, strengite, scorodite and mansfieldite**

**J. Theo Kloprogge<sup>12\*</sup> and Barry J. Wood<sup>3</sup>**

<sup>1</sup> School of Earth and Environmental Sciences, The University of Queensland, Brisbane,  
Qld 4072, Australia

<sup>2</sup> Department of Chemistry, College of Arts and Sciences, University of the Philippines  
Visayas, Miagao, Iloilo, Philippines

<sup>3</sup> Centre for Microscopy & Microanalysis, The University of Queensland, Brisbane, Qld  
4072, Australia

**\*Email: [j.kloprogge@uq.edu.au](mailto:j.kloprogge@uq.edu.au)**

**Running title:** XPS and Raman spectroscopy of variscite group minerals

---

**ABSTRACT**

Several structurally related  $\text{AsO}_4$  and  $\text{PO}_4$  minerals, were studied with Raman microscopy and X-ray Photoelectron Spectroscopy (XPS). XPS revealed only Fe, As and O for scorodite. The Fe 2p, As 3d, and O 1s indicated one position for  $\text{Fe}^{2+}$ , while 2 different environments for O and As were observed. The O 1s at 530.3 eV and the As 3d 5/2 at 43.7 eV belonged to  $\text{AsO}_4$ , while minor bands for O 1s at 531.3 eV and As 3d 5/2 at 44.8 eV were due to  $\text{AsO}_4$  groups exposed on the surface possibly forming OH-groups. Mansfieldite showed, besides Al, As and O, a trace of Co. The  $\text{PO}_4$  equivalent of mansfieldite is variscite. The change in crystal structure replacing As with P resulted in an increase in the binding energy (BE) of the Al 2p by 2.9 eV. The substitution of  $\text{Fe}^{3+}$  for  $\text{Al}^{3+}$  in the structure of strengite resulted in a Fe 2p at 710.8 eV. An increase in the Fe 2p BE of 4.8 eV was found between mansfieldite and strengite. The scorodite Raman OH-stretching region showed a sharp band at  $3513\text{ cm}^{-1}$  and a broad band around  $3082\text{ cm}^{-1}$ . The spectrum of mansfieldite was like that of scorodite with a sharp band at  $3536\text{ cm}^{-1}$  and broader maxima at  $3100\text{ cm}^{-1}$  and  $2888\text{ cm}^{-1}$ . Substituting Al in the arsenate structure instead of Fe resulted in a shift of the metal-OH-stretching mode by  $23\text{ cm}^{-1}$  towards higher wavenumbers due to a slightly longer H-bonding in mansfieldite compared to scorodite. The intense band for scorodite at  $805\text{ cm}^{-1}$  was ascribed to the symmetric stretching mode of the  $\text{AsO}_4$ . The medium intensity bands at 890, 869, and  $830\text{ cm}^{-1}$  were ascribed to the internal modes. A significant shift towards higher wavenumbers was observed for mansfieldite. The strengite Raman spectrum in the  $900\text{-}1150\text{ cm}^{-1}$  shows a strong band at  $981\text{ cm}^{-1}$  accompanied by a series of less intense bands. The  $981\text{ cm}^{-1}$  band was assigned to the  $\text{PO}_4$  symmetric stretching mode, while the weak band at  $1116\text{ cm}^{-1}$  was the corresponding antisymmetric stretching mode. The remaining bands at 1009, 1023 and  $1035\text{ cm}^{-1}$  were assigned to  $\nu_1(\text{A}_1)$  internal modes in analogy to the interpretation of the  $\text{AsO}_4$  bands for scorodite and mansfieldite. The variscite spectrum showed a shift towards higher

wavenumbers in comparison to the strengite spectrum with the strongest band observed at  $1030\text{ cm}^{-1}$  and was assigned to the symmetric stretching mode of the  $\text{PO}_4$ , while the corresponding antisymmetric stretching mode was observed at  $1080\text{ cm}^{-1}$ . Due to the band splitting component bands were observed at  $1059$ ,  $1046$ ,  $1013$  and  $940\text{ cm}^{-1}$ . The  $\text{AsO}_4$  symmetric bending modes for scorodite were observed at  $381$  and  $337\text{ cm}^{-1}$ , while corresponding antisymmetric bending modes occurred at  $424$ ,  $449$  and  $484\text{ cm}^{-1}$ . Comparison with other arsenate and phosphate minerals showed that both XPS and Raman spectroscopy are fast and non-destructive techniques to identify these minerals based on their differences in chemistry and the arsenate/phosphate vibrational modes due to changes in the symmetry and the unique fingerprint region of the lattice modes.

**Keywords:** Raman Spectroscopy; scorodite; strengite; variscite; mansfieldite; X-ray Photoelectron Spectroscopy

## Introduction

The variscite group of minerals have a general formula of  $ATO_4 \cdot 2H_2O$  where, A is Al,  $Fe^{3+}$ , Sc or other trivalent cations and T is P or As. The structure is orthorhombic in space group  $Pbca$  or is monoclinic in space group  $P2_1/n$ . The structure can be envisaged as being built of alternate  $TO_4$  tetrahedra and octahedrally coordinated cations that associate in a three-dimensional network. The trivalent cations have a distorted octahedral coordination with O from four  $TO_4$  groups and O from two water molecules [1, 2].

Though scorodite can be found as a primary mineral at hydrothermal deposits such as at Saubach, Vogtland, Germany, most of the scorodite is formed as the oxidation product of arsenopyrite or other As-bearing sulphides (realgar, orpiment, cobaltite, enargite, gersdorffite, löllingite, and As-bearing pyrite and tennantite); see e.g. [1, 3-8]. The mobility of arsenic due to leaching from these primary arsenic minerals in mine tailings into soils and groundwater and the formation of secondary arsenate minerals has been the subject of numerous studies [9-35]. The decomposition in water of arsenic containing waste solids depends strongly on the crystallinity and the type of arsenic-bearing phases. It is well established that both scorodite and mansfieldite have significantly lower solubilities compared to their amorphous counterparts [36-38]. The formation of scorodite with its low solubility is one of the methods either through direct deposition or through bioformation using bacteria which has received considerable interest in recent years [12, 13, 15, 23, 39-42].

Scorodite is one of the minerals in the variscite group where it forms series with both mansfieldite ( $AlAsO_4 \cdot 2H_2O$ ) and yanomamite ( $InAsO_4 \cdot 2H_2O$ ) and is dimorphous with parascorodite. It is probable that a complete solid solution exists between scorodite and mansfieldite similar to that of variscite and strengite. Scorodite was named in 1818 by Johann Friedrich August Breithaupt from the Greek σκορόδιου = "Scorodion" – garlic-like, in allusion to its odour when heated [43]. It crystallises in the orthorhombic system, point group

2/m 2/m 2/m. The space group is  $Pcab$  with  $a = 9.996 \text{ \AA}$ ,  $b = 10.278 \text{ \AA}$ ,  $c = 8.397 \text{ \AA}$ . Most commonly it is found as crystalline crusts but crystals can form up to 5 cm in size. Crystals tend to be pyramidal [44], tabular [001], or prismatic [010] with large {111}, {101}, {201} and/or {001}. The colour varies from almost colourless to pale blue-green, greyish blue, brownish yellow, translucent with a vitreous to subadamantine lustre [45].

Mansfieldite,  $\text{AlAsO}_4 \cdot 2\text{H}_2\text{O}$ , was named in 1948 after George Rogers Mansfield (1875-1947), former Chief of the Section of Areal and non-metalliferous Geology of the U.S. Geological Survey [46]. Similar to scorodite it crystallises in the space group  $Pcab$  with  $a = 9.996 \text{ \AA}$ ,  $b = 10.278 \text{ \AA}$  and  $c = 8.937 \text{ \AA}$ . Crystals tend to be pyramidal {111}, tabular {001} or prismatic [010]. It is often found as aggregates or crusts with massive or porous and sinter-like or earthy habit. The colour can vary from pale leek-green to liver-brown, colourless, bluish, violet or yellow. Earthy material is generally pale green to greyish green or brownish green. The lustre varies from vitreous to subadamantine or subresinous.

Variscite and strengite form the two phosphate end-members with a complete solid solution between  $\text{Fe}^{3+}$  and Al. Variscite,  $\text{AlPO}_4 \cdot 2\text{H}_2\text{O}$ , was named in 1837 for Variscia, the ancient name for Voigtland in Germany [47]. It crystallises in the space group  $Pbca$  with  $a = 9.822 \text{ \AA}$ ,  $b = 8.558 \text{ \AA}$  and  $c = 9.622 \text{ \AA}$ . Most commonly it is found as massive coatings or cryptocrystalline aggregates, fine-grained masses or nodules of pale to emerald-green colour and vitreous to waxy lustre. Variscite occurs as precipitations from circulating water in near surface cavities or as a hydrothermal mineral in ultra-alkaline pegmatites, often associated with a series of other more exotic phosphates such as crandallite, fluorapatite, wardite, millisite, gordonite, montgomeryite, overite, kolbeckite, goyazite, etc. [48, 49]. Strengite,  $\text{FePO}_4 \cdot 2\text{H}_2\text{O}$ , was named after Johann August Streng (1830-1897), an at that time well-known mineralogist from the University of Giessen in Germany by his former student August Nies [1, 50]. It also crystallises in the space  $Pbca$  but with a slightly larger unit cell with  $a =$

10.07 Å,  $b = 9.82$  Å and  $c = 8.67$  Å. Strengite tends to form spherical or botryoidal aggregates with radial fibrous structure with peach-blossom red, carmine or violet colour. Strengite is a late secondary mineral in complex granite pegmatites, often formed by alteration of triphyllite,  $\text{LiFe}^{2+}\text{PO}_4$ , and other pegmatitic phosphates [48]. The formation of both these phosphates in colloidal form in soils may play an important role in the release of phosphorus into the soil solution and subsequent uptake of phosphorus by plants. These colloidal phosphates can be formed through erosion and weathering of existing phosphate rocks through a process of dissolution and precipitation [51], but are more likely to be formed through the accumulation of rock phosphates in soils [52, 53]. In contrast, excessive fertilizer use can result in the precipitation of these minerals at high soil P concentrations acting as a sink for P that has a constant solubility under given chemical and physical conditions [54].

Whilst some X-ray Photoelectron, infrared, and Raman spectroscopic data have been reported more work is needed on these important minerals [2, 3, 55-65]. As part of an ongoing study on arsenate minerals [66-72] this study aims at a better understanding of the XPS and Raman spectrum of well crystallised variscite group minerals. A better understanding of the Raman spectrum of variscite, strengite, scorodite and mansfieldite will help with the identification of these important secondary minerals in e.g. soils as a result of leaching from mine tailings.

## **Experimental**

### *Sample origin*

The variscite sample came from Dug Hill, Avant, Garland Co., Arkansas, U.S.A. catalogued under number 270383012 in personal collection of the first author. The strengite came from the Silbergrube (Silver Mine or Quarry), Waidhaus, Vohenstrauß, Oberpfälzer Wald, Upper Palatinate, Bavaria, Germany and forms part of the first author's private micromount



collection under catalogue number 3026. This strengite specimen shows an association with laueite and phosphosiderite. The scorodite used in this study is part of the first author's private micromount collection under catalogue number 030107073 and originates from the Hemerdon Mine (also known as the Hemerdon Bal Mine or Hemerdon Ball Mine), Plympton, Tavistock District, Devon, UK. The specimen consists of small distinct crystals of light bluish green colour up to about 2 mm in size. The mansfieldite sample used in this study is part of the first author's private micromount collection under catalogue number 8472 and originates from the Mount Cobalt Mine, Selwyn District, Mount Isa-Cloncurry area, Queensland, Australia. It consists of distinct light purple mansfieldite crystals accompanied by straw-yellow smolianinovite.

#### *X-ray Photoelectron Spectroscopy (XPS)*

The XPS analyses were performed on a Kratos AXIS Ultra with a monochromatic Al X-ray source at 225 W under ultrahigh vacuum conditions. Each analysis started with a survey scan from 0 to 1200 eV with a dwell time of 100 milliseconds, pass energy of 160 eV at steps of 1 eV with 1 sweep. For the high resolution analysis the number of sweeps was increased, the pass energy was lowered to 20 eV at steps of 100 meV and the dwell time was changed to 250 milliseconds. The spectra were charge corrected using the advantageous C 1s signal at 284.8 eV. The sample with the crystal in situ was placed in the XPS after a wash with alcohol. Prior to the analyses the surface of the crystal was cleaned by etching for 20 minutes.

#### *Raman microscopy*

The samples were orientated on a polished metal surface on the stage of an Olympus BHSM microscope equipped with 10x and 50x objectives. The microscope is part of a Renishaw

1000 Raman microscope system, which also includes a monochromator, a filter system and a Charge Coupled Device (CCD). The Raman spectra were excited by a Spectra-Physics model-127 H-Ne laser producing highly polarised light at 633 nm. Spectra were obtained at a nominal resolution of  $2\text{ cm}^{-1}$  and a precision of around  $1\text{ cm}^{-1}$ . Laser power was kept low at about 10% in order to prevent any chance of phase transformations/radiation damage to occur on the surface of the crystals studied. Lower laser power measurements did not show any differences compared to this laser power setting. Spectroscopic manipulation such as baseline adjustment, smoothing and normalisation were performed using the Fityk 0.9.8 software package, which enabled the type of fitting, function to be selected and allows specific parameters to be fixed or varied accordingly [73]. Band fitting was done using a Gauss-Lorentz cross-product function with the minimum number of component bands used for the fitting process. The Gauss- Lorentz ratio was maintained at values greater than 0.7 and fitting was undertaken until reproducible results were obtained with squared correlations of  $r^2$  greater than 0.995.

## Results and discussion

Chemical information about the scorodite was obtained from the XPS surface scan (Fig. 1), which showed only the presence of C (surface contamination still present even after 20 minutes etching), O, As, and Fe (Table 1). No traces of other elements were observed. The analysis was very close to the theoretical values based on  $\text{Fe}_2\text{AsO}_4$ , i.e. Fe 2: As 1: O 4.

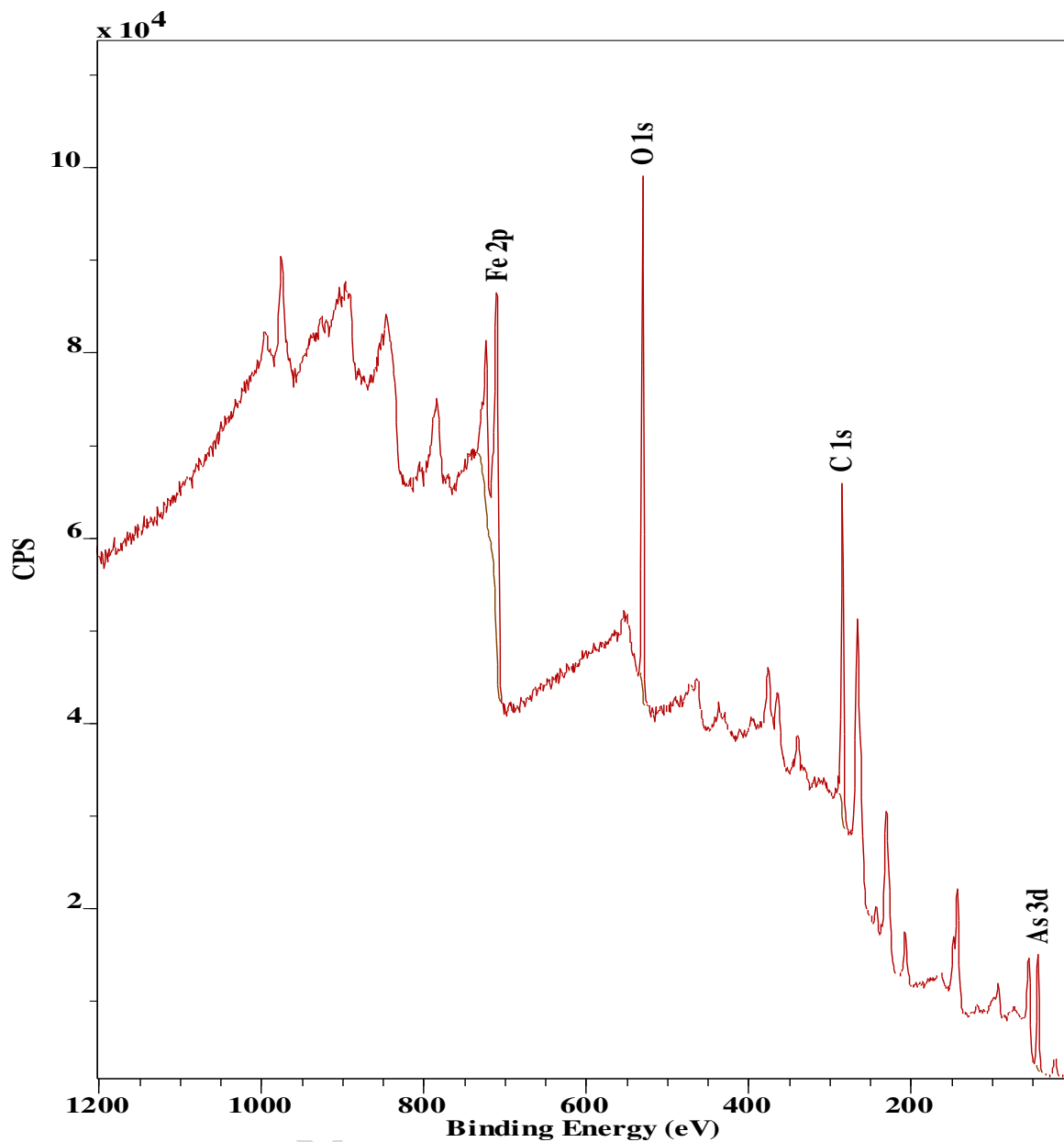


Figure 1 XPS survey scan (Al  $K\alpha$ , 225 W, 160 eV pass energy) of scorodite

Table 1 Chemical composition of the scorodite based on XPS analysis.

Element	Atom%	Theoretical atom%
O	54.1	57.1
Fe	31.3	28.6
As	14.5	14.3

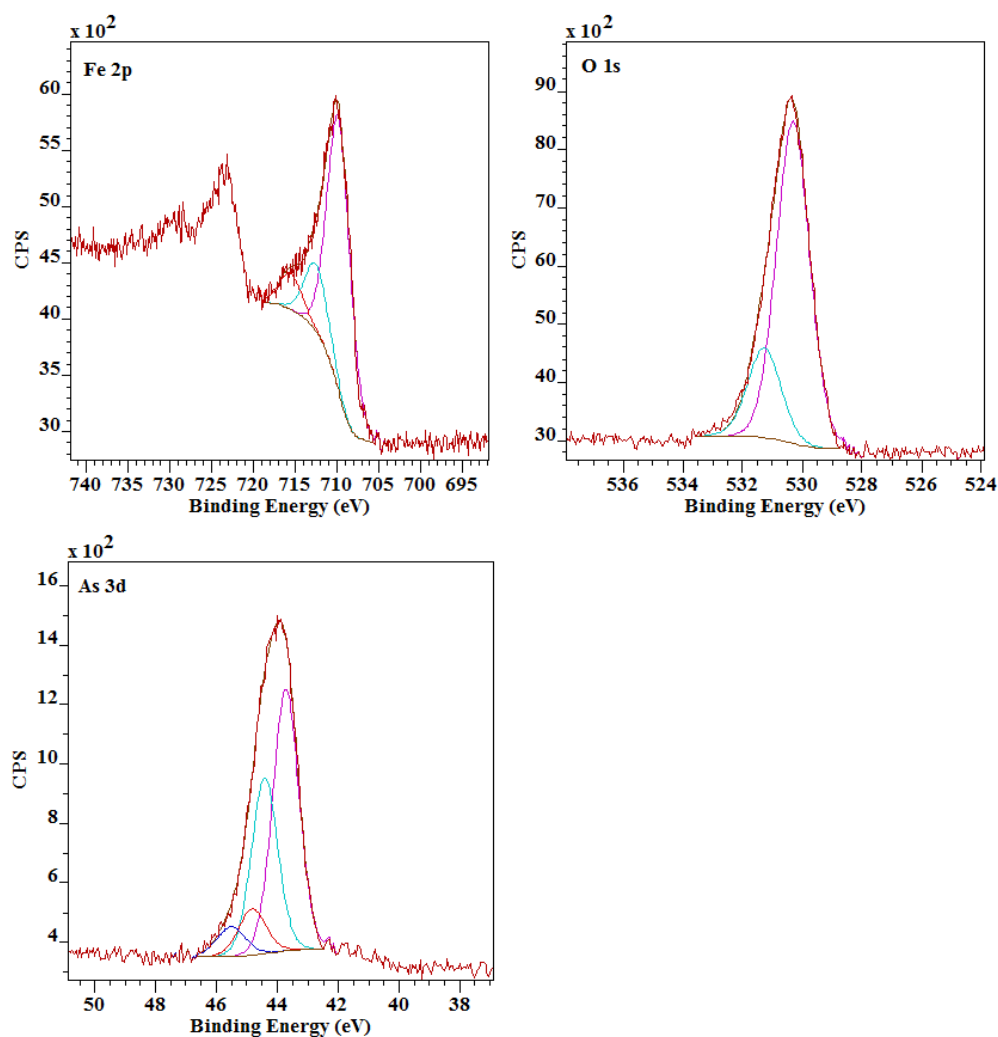


Figure 2 High resolution XPS spectra (Al K $\alpha$ , 150 W, 20 eV pass energy) of scorodite

The Fe 2p high resolution spectrum showed a single contribution at 709.7 eV with shake up satellite bands at slightly higher binding energies of 712.5 and 715.5 eV (Fig. 2). The position and the fact that only a single signal was observed is in agreement with the fact that only a single metal position is present in the scorodite structure and that the iron is present in the Fe<sup>2+</sup> state. Frau et al. [44] referred in their paper to unpublished results for scorodite, where the Fe 2p was observed at a slightly higher binding energy of 712 eV.

The corresponding O 1s spectrum exhibited two bands, an intense band at 530.3 eV and lower intensity band at 531.3 eV (Fig. 2). This indicates that two different oxygen species are present at the surface of the scorodite crystal. Based on earlier work the band at 530.3 eV is associated with the  $\text{AsO}_4$  group in the scorodite crystal structure, while the smaller band at slightly higher binding energy is possibly associated with  $\text{H}_2\text{O}$  groups [74]. The observed ratio of 3:1 is slightly lower than the theoretical value of 2:1 and is possibly caused by partial dehydration under the ultra-high vacuum conditions. An alternative explanation is that the scorodite is locally dehydrated and the band is due to the formation of hydroxyl groups at the surface in the form of  $\text{AsO}_{4-x}(\text{OH})_x$ . This second hypothesis is supported by the fact that the observed ratio of O to Fe and As is 4 to 2 to 1 (Table 1), whereas a fully hydrated scorodite would have a ratio of 6 to 2 to 1.

The binding energies of the As 3d ranged from 43.7 to 44.8 eV which is typical for compounds with As(V) bound to oxygen in  $\text{AsO}_4$ -bearing phases [44]. Two different arsenic species were observed with the most intense As 3d 5/2 band at 43.7 eV associated with the  $\text{AsO}_4$  group in the normal scorodite crystal structure, whereas the lesser intensity As 3d 5/2 band at a slightly higher binding energy of 44.8 eV was associated with  $\text{AsO}_4$  groups exposed at the surface of the crystal, where it could possibly form hydroxyl groups or react with the remaining carbon still present on the surface. The fact that two arsenic bands were observed would make the second explanation for the second O 1s band being due to surface hydroxyls more plausible.

The mansfieldite survey spectrum showed, besides the expected bands for Al, As and O, the presence of a small amount of Co (Fig. 3). Previous work has established that the purple colour of the mansfieldite from this locality, which also produces the cobalt arsenate mineral erythrite, is due to the substitution of some Co in the mansfieldite structure. The atom percentages are 0.93 at% Al and 0.07 at% Co. The ratio of (Al+Co) to As of 0.985 is very

close to the theoretical value of 1. The ratio of O to As of 4.74 indicates that similar to what was observed for scorodite, local partial dehydration was caused by the combined effects of etching and ultrahigh vacuum.

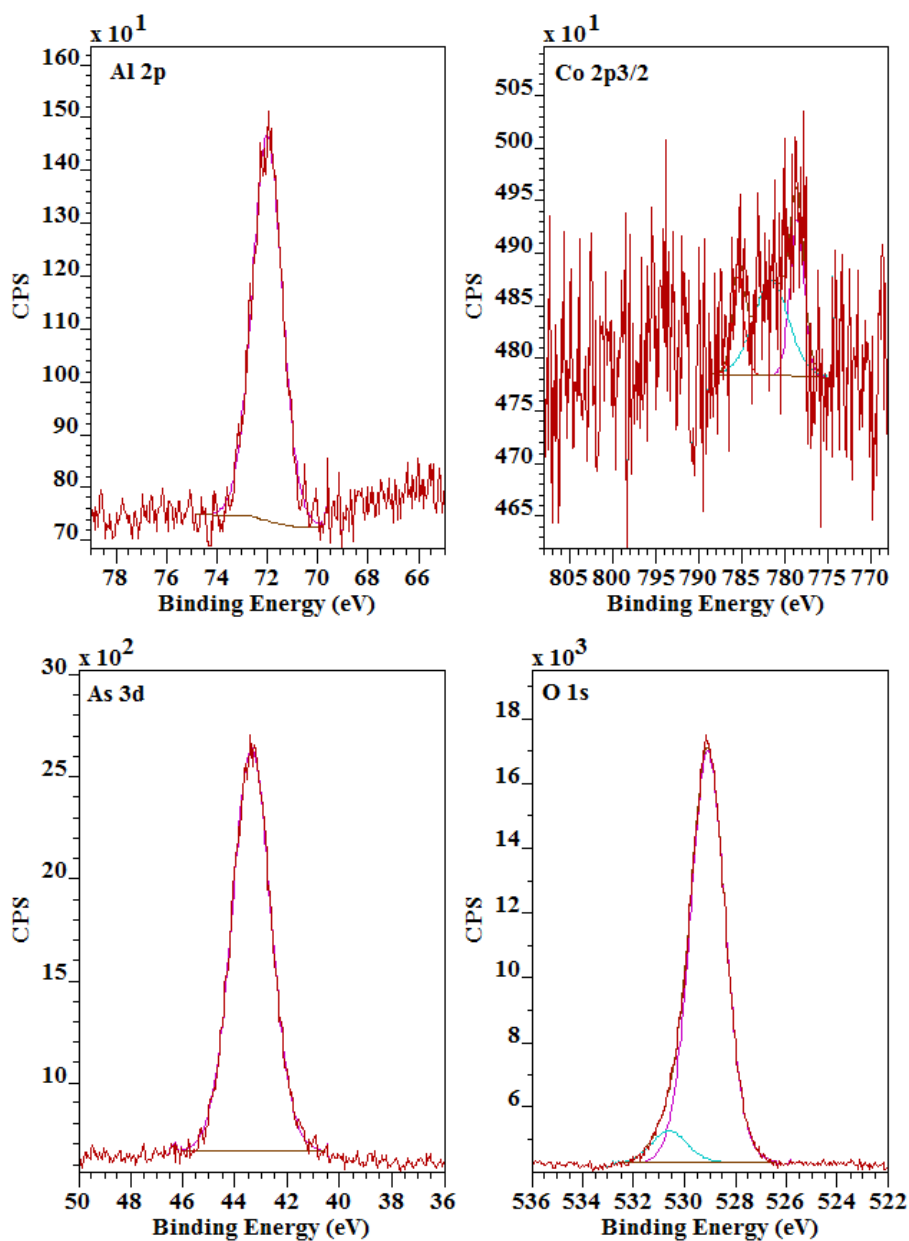


Figure 3 High resolution XPS spectra (Al K $\alpha$ , 150 W, 20 eV pass energy) of mansfieldite

The Al 2p showed a single band with a binding energy of 72.0 eV, which is significantly lower than for example Al hydroxides that have binding energies around 74 eV [74]. Similar to the Fe 2p in scorodite the observation of only a single band confirms the

existence of only a single Al position in mansfieldite. The corresponding Co 2p 3/2 was observed at 778.6 eV together with some shake up satellite bands at higher binding energies. The substitution of Fe<sup>3+</sup> by Al resulted in a small shift of about 1 eV to lower binding energies for the O 1s to 529.1 eV and 530.6 eV with a ratio of about 12.8 to 1 indicative of a much stronger partial dehydration than that observed for scorodite. The As 3d also shifted slightly towards lower binding energies with the As 3d 5/2 bands at 42.6 eV and 43.4 eV with the corresponding Ad 3d 3/2 bands at 43.3 eV and 44.1 eV.

The phosphate equivalent of mansfieldite is the mineral variscite. The Al 2p is characterised by a single band with a binding energy of 74.9 eV (Fig. 4). The change in the crystal structure replacing the arsenate group by the phosphate group results in a significant increase in the binding energy of the Al 2p by as much as 2.9 eV. The corresponding P 2p exhibited a single band at 134.5 eV. The O 1s cannot be interpreted in a similar way as was done for the scorodite and mansfieldite because the silicate background upon which the thin layer of variscite is sitting attributed to the overall O 1s signal. Two distinct bands can be observed at 531.6 eV and 532.6 eV but it is impossible to assign the bands with certainty to the variscite. However, comparison with the mansfieldite O 1s does show that both bands are observed at higher binding energies in line with the shift to a higher binding energy for the Al 2p.

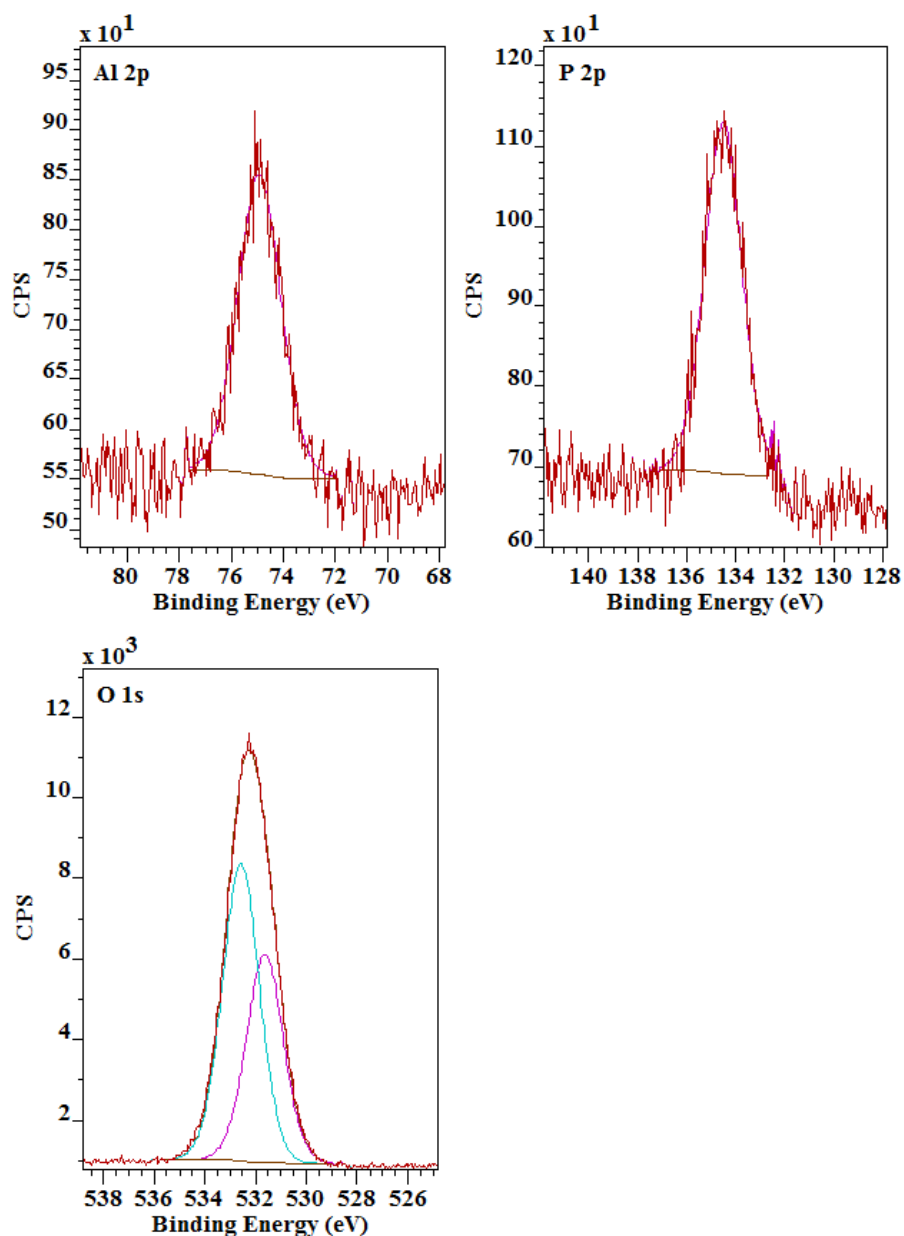


Figure 4 High Resolution XPS (Al K $\alpha$ , 150 W, 20 eV pass energy) of variscite

The substitution of Fe<sup>3+</sup> for Al in the structure of the phosphate strengite resulted in a Fe 2p band at 710.8 eV with a shake-up satellite band at 714.5 eV (Fig. 5). Similar to the increase in binding energy for the Al 2p between scorodite and variscite, an increase in the Fe 2p binding energy of 4.8 eV is observed between mansfieldite and strengite. The P 2p was observed at 133.9 eV, which is 0.6 eV lower than in variscite. This is in contrast to the shift observed for the arsenates scorodite and mansfieldite, where a small shift to higher binding



energies was observed. The O 1s is complex showing multiple bands due to the interference of quartz mixed in with the strengite. Two strong bands were observed at 531.6 and 532.8 eV with a minor band at 534.0 eV. Based on earlier published results of O 1s values around 533 eV for quartz it is reasonable to assign the band at 532.8 eV to quartz and the remaining two bands to strengite [75, 76]. In line with the shift of the O 1s to higher binding energies observed for variscite, here also a shift to higher binding energies is observed compared to its arsenate analogue scorodite.

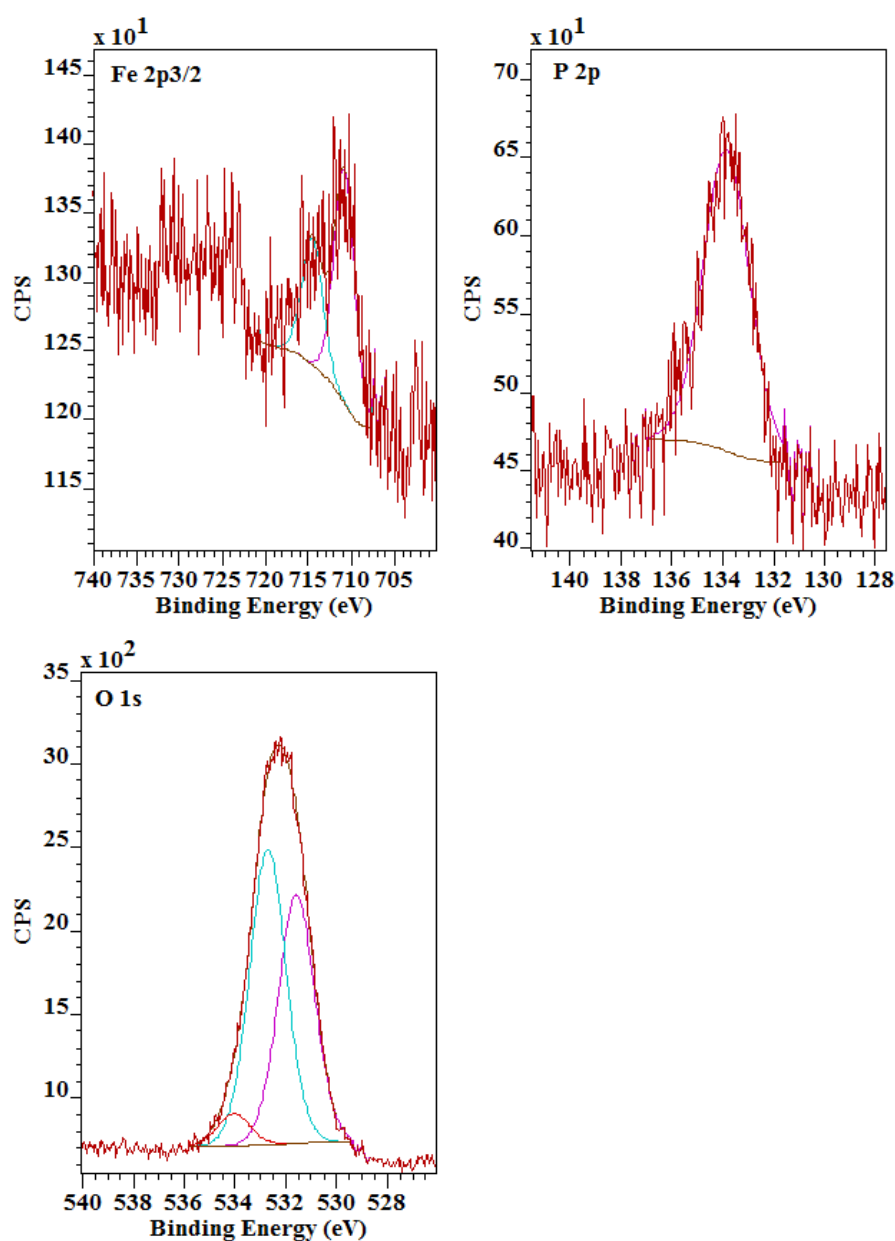


Figure 5 High Resolution XPS (Al K $\alpha$ , 150 W, 20 eV pass energy) of strengite

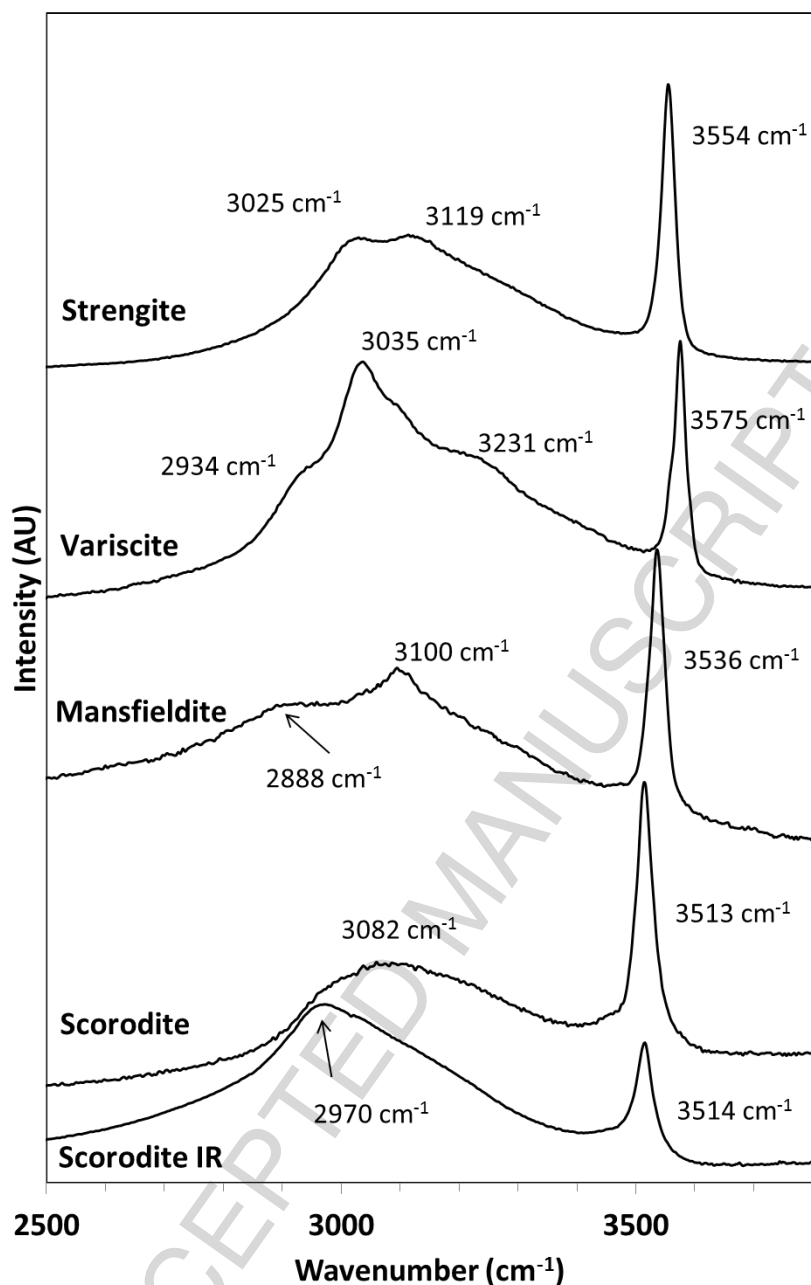


Figure 6 The OH-stretching region between 2500 and 3800 cm<sup>-1</sup> showing the Raman spectra of scorodite, mansfieldite, variscite and strengite. For comparison the IR spectrum of scorodite is shown.

The hydroxyl stretching region between 3000 and 400 cm<sup>-1</sup> showed a sharp band at 3513 cm<sup>-1</sup> and a broad band around 3082 cm<sup>-1</sup> in the Raman spectrum for scorodite with corresponding bands in the mid-infrared spectrum at 3514 cm<sup>-1</sup> and 2970 cm<sup>-1</sup> with

asymmetric tail at higher wavenumbers, indicating that the broad band in the Raman probably contains more than one hydroxyl stretching mode (Fig. 6). In earlier work similar bands were observed by e.g. Baghurst, Barrett, Coleyshaw, Griffith and Mingos [62] at 3511  $\text{cm}^{-1}$  (sharp) and 2927  $\text{cm}^{-1}$  (broad) and Ondrus, Skala, Viti, Veselovsky, Novak and Jansa [55] at 3516  $\text{cm}^{-1}$  (sharp) and 2969 and 3300  $\text{cm}^{-1}$  (broad) in the infrared spectrum and Gomez, Assaaoudi, Becze, Cutler and Demopoulos [59] at 3516  $\text{cm}^{-1}$  (sharp) and 3080  $\text{cm}^{-1}$  (broad) in the Raman spectrum and at 3516  $\text{cm}^{-1}$  and 2960  $\text{cm}^{-1}$  in the infrared spectrum. In contrast, Filippi, Machovic, Drahota and Bohmova [56] reported a rather different Raman spectrum with the characteristic sharp band at 3514  $\text{cm}^{-1}$  but associated with two broader bands at 3427  $\text{cm}^{-1}$  and 3600  $\text{cm}^{-1}$ . Since the scorodite in their sample was part of a more complex system in nodules of arsenopyrite associated with secondary minerals such as kaňkite ( $\text{Fe}^{3+}\text{AsO}_4 \cdot 3.5\text{H}_2\text{O}$ ), native sulphur and pitticite (amorphous iron arsenate), it is probable that another phase contributed to the observed spectrum.

The two bands are associated with hydroxyl stretching vibrations of water molecules in the crystal structure of scorodite, where they are bonded to iron octahedral and are sitting in a tunnel structure along the c-axis [63]. The hydroxyl nature of these bands was confirmed by Baghurst, Barrett, Coleyshaw, Griffith and Mingos [62], who showed that after deuteration these two bands shifted to 2605 and 2236  $\text{cm}^{-1}$  in the infrared and 2612 and 2264  $\text{cm}^{-1}$  in the Raman spectrum, respectively.

These two vibrations can be correlated to two distinct types of hydrogen bonding that occur in the crystal structure of scorodite between the water molecules and the arsenate group. The broad OH-stretching band can be associated with a strong type of hydrogen bonding (shorter O-H bond length) that occurs with the arsenate groups. The sharp OH-stretching band can be associated with the weaker hydrogen bonding (longer O-H bond length) between the oxygen atoms [36, 63].

The hydroxyl-stretching region in the Raman spectrum of mansfieldite was very similar to that of scorodite with a sharp band at  $3536\text{ cm}^{-1}$  and a broader feature at lower wavenumbers with distinct maxima at  $3100\text{ cm}^{-1}$  and  $2888\text{ cm}^{-1}$ . Similar bands were observed by Gomez, Le Berre, Assaoudi and Demopoulos [77] at  $3534\text{ cm}^{-1}$  (sharp) and  $3105\text{ cm}^{-1}$  and  $2888\text{ cm}^{-1}$  (broad). As a result of substituting Al in the arsenate structure instead of iron a significant shift of the sharp band associated with the metal-hydroxyl group of  $23\text{ cm}^{-1}$  towards higher wavenumbers was observed. This shift is associated with a slightly longer H-bonding in mansfieldite compared to that in scorodite [77]. A similar effect was observed in the corresponding phosphates strengite and variscite with a shift from  $3554\text{ cm}^{-1}$  to  $3575\text{ cm}^{-1}$  ( $21\text{ cm}^{-1}$  shift). Ross [78] reported a shift of  $23\text{ cm}^{-1}$  from  $3565\text{ cm}^{-1}$  to  $3588\text{ cm}^{-1}$  in the infrared spectra, while Frost, Weier, Erickson, Carmody and Mills [79] reported a series of infrared bands but no Raman bands in a table at 3580, 3564, 3282, 3094, 3059, 2945 and  $2910\text{ cm}^{-1}$  without further explanation or discussion how these bands were obtained or what their physical meaning is in terms of different OH-stretching vibrations allowed within the crystal structure of variscite and no bands at all were reported for strengite. Strengite and variscite show evidence of three broad bands around 3025, 3119 (and possibly 3250)  $\text{cm}^{-1}$  for strengite and 2934, 3035 and  $3231\text{ cm}^{-1}$  for variscite, respectively. Based on a crystal structure only containing  $2\text{H}_2\text{O}$  or  $(\text{H}_3\text{O})^+(\text{OH})^-$  only two hydroxyl stretching modes would be expected. Since the sharp band around  $3515\text{-}3575\text{ cm}^{-1}$  for all four minerals is associated with the (Fe,Al)-OH stretching mode, a plausible explanation for the occurrence of three broad bands at lower wavenumbers are associated with two different types of  $\text{H}_2\text{O}$  plus  $\text{H}_3\text{O}^+$  showing different O-H bonds both present instead of in the earlier literature assumed presence of either  $2\text{H}_2\text{O}$  or  $(\text{H}_3\text{O})^+(\text{OH})^-$ . Based on Fig. 6, these different types are better defined in strengite and variscite than in scorodite and mansfieldite.

The vibrational modes of arsenate anions in aqueous solutions are reasonably well known with the symmetric stretching vibration  $\nu_1(A_1)$  around  $810\text{ cm}^{-1}$  coinciding with the antisymmetric  $\nu_3(F_2)$  mode around  $790\text{ cm}^{-1}$ . The symmetric bending mode  $\nu_2(E)$  is observed around  $340\text{ cm}^{-1}$  and the antisymmetric bending mode  $\nu_4(F_2)$  around  $400\text{ cm}^{-1}$ . Of these four modes the  $F_2$  modes are Raman active and infrared active, while the  $A_1$  and  $E$  modes are Raman active only. Earlier work by Myneni, Traina, Waychunas and Logan [64] has shown that the  $T_d$  symmetry of the arsenate tetrahedron is hardly ever preserved in crystals because of its strong affinity to protonate, hydrate, and complex with metal ions. As a result the symmetry will be reduced to either  $C_{3v}/C_3$  (corner sharing),  $C_{2v}/C_2$  (edge-sharing, bidentate binuclear) or  $C_1/C_s$  (corner sharing, edge sharing, bidentate binuclear, multidentate). The effect of reduced site symmetry in a crystal will remove the degeneracy and allow activation of all vibrations in the infrared and Raman spectra and splitting of the bands. Furthermore the vibrational spectrum, in this study Raman only, is also composed of lattice modes, generally below  $300\text{ cm}^{-1}$ .

Within the crystal structure of scorodite and mansfieldite both water and arsenate molecules occupy  $C_1$  symmetry sites. According to the corresponding factor group analysis for the arsenate this leads to:  $\Gamma(\text{AsO}_4^{3-}) = 9(A_g(\text{Ra}) + B_{1g}(\text{Ra}) + B_{2g}(\text{Ra}) + A_u(\text{In.}) + B_{1u}(\text{IR}) + B_{2u}(\text{IR}) + B_{3u}(\text{IR}))$ .

Table 2 Spectral predictions and correlation schemes for the internal modes of  $\text{TO}_4^{3-}$  in  $\text{M}^{3+}\text{TO}_4 \cdot 2\text{H}_2\text{O}$  with  $T = \text{As}$  or  $\text{P}$ .

Free ion symmetry	Site symmetry	Factor group symmetry
$T_d$	$C_1$	$D_{2h}$
$A_1$	$9 A$	$9 A_g (\text{R})$
$E$		$9 B_{1g} (\text{R})$
$2T_2$		$9 B_{2g} (\text{R})$
		$9 B_{3g} (\text{R})$
		$9 A_u (\text{In.})$
		$9 B_{1u} (\text{IR})$
		$9 B_{2u} (\text{IR})$
		$9 B_{3u} (\text{IR})$

R = Raman; IR = Infrared.

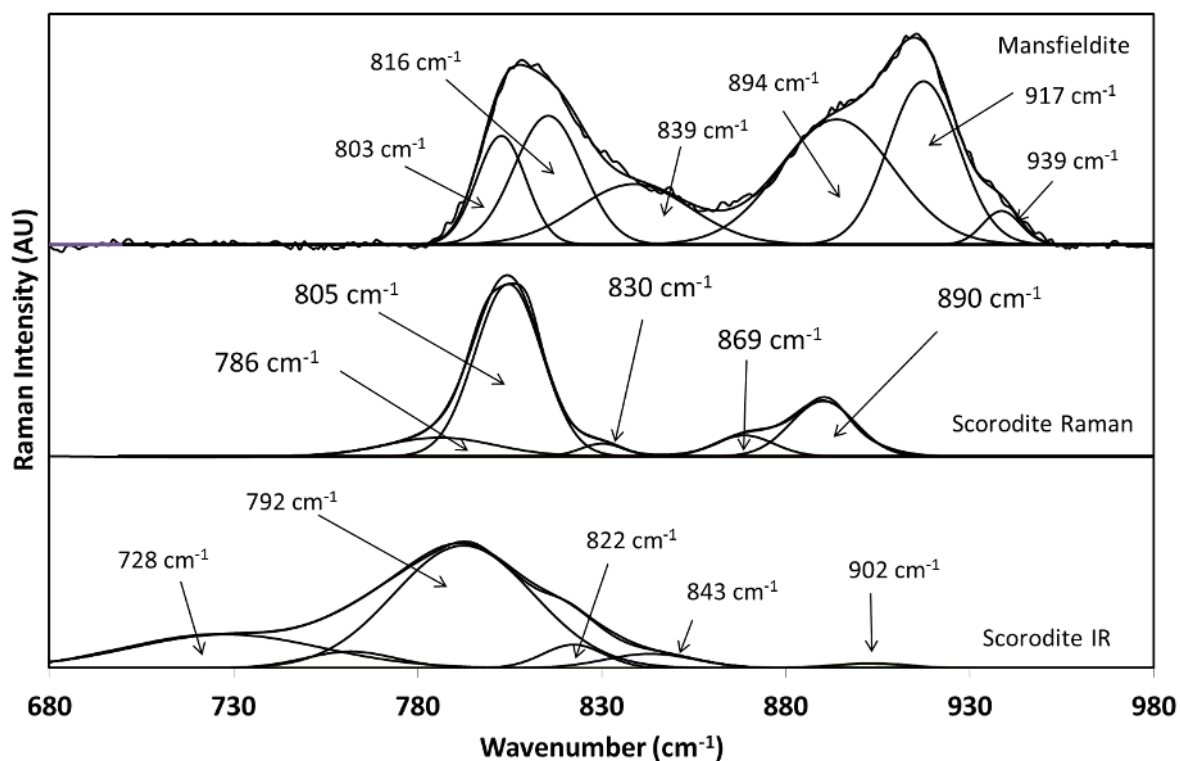


Figure 7 Raman spectra of scorodite and mansfieldite in the 680-980  $\text{cm}^{-1}$  region. For comparison the IR spectrum of scorodite is also given.

Figure 7 shows the Raman spectra of scorodite and mansfieldite plus the mid-infrared spectrum of scorodite in the region between 680 and 980  $\text{cm}^{-1}$ . The most intense band for scorodite at 805  $\text{cm}^{-1}$  could be ascribed to the symmetric stretching vibration of the arsenate anion. The corresponding IR band occurs at 792  $\text{cm}^{-1}$ . A similar band was observed at 800  $\text{cm}^{-1}$  in the Raman and 705  $\text{cm}^{-1}$  in the infrared by Gomez, Assaoudi, Becze, Cutler and Demopoulos [59]. The three medium intensity band at higher wavenumbers (890, 869, and 830  $\text{cm}^{-1}$ ) could be ascribed to the internal modes in accordance with the findings of Gomez, Assaoudi, Becze, Cutler and Demopoulos [59], who observed similar bands at 880, 870 and 830  $\text{cm}^{-1}$ . Corresponding bands in the infrared spectrum were observed around 902, 843 and 822  $\text{cm}^{-1}$ . Different from their findings is the observation of a weak band at 786  $\text{cm}^{-1}$  which

could be ascribed to the OH bending mode. Savage, Bird and O'Day [80] assigned the band at about  $800\text{ cm}^{-1}$  to an antisymmetric stretching mode associated with oxygen bridging between As and Fe (As-O-Fe) and a smaller band at  $893\text{ cm}^{-1}$  to a non-bridging oxygen that may be associated with crystal edges or defects. A shoulder at  $831\text{ cm}^{-1}$  was assigned to the As-OFe symmetrical stretching mode and not to the antisymmetric stretching mode of the arsenate anion.

A significant shift towards higher wavenumbers was observed for mansfieldite and the interpretation is not as straightforward as for scorodite. The only publication on the Raman spectrum of mansfieldite by Gomez, Le Berre, Assaaoudi and Demopoulos [77] interpret the arsenate symmetric stretching mode at  $918\text{ cm}^{-1}$ . Even though a similar band was observed at  $917\text{ cm}^{-1}$ , it seems unlikely that the substitution of Fe by Al in the structure would result in a shift of more than  $100\text{ cm}^{-1}$ . However, based on the similarities between the spectra of scorodite and mansfieldite an alternative and more consistent interpretation is that the band at  $816\text{ cm}^{-1}$  is the symmetric stretching mode with only a shift of  $11\text{ cm}^{-1}$  and the bands at  $939, 917, 894,$  and  $839\text{ cm}^{-1}$  as the internal modes and the band at  $803\text{ cm}^{-1}$  as the equivalent of the band at  $786\text{ cm}^{-1}$  for scorodite.

Similar to the vibrational modes of the arsenate anions, the phosphate anions are also well known. Four types of vibrations can be observed: the symmetric stretching mode  $\nu_1(A_1)$  mode  $980\text{ cm}^{-1}$ , the antisymmetric stretching mode  $\nu_3(F_2)$  around  $1080\text{ cm}^{-1}$ , the symmetric bending mode  $\nu_2(E)$  around  $360\text{ cm}^{-1}$  and the antisymmetric bending mode  $\nu_4(F_2)$  around  $500\text{-}515\text{ cm}^{-1}$  [78]. Of these modes the  $F_2$  modes are Raman and infrared active, while the  $A_1$  and E modes are Raman active only.

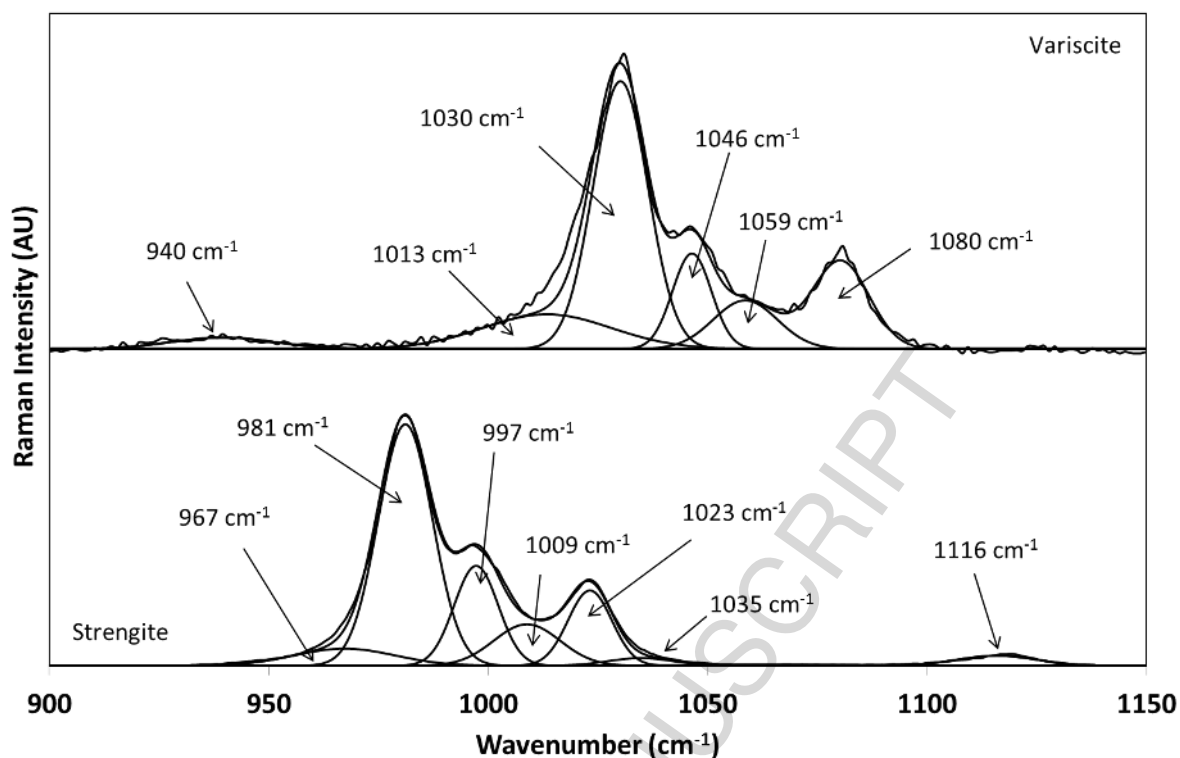


Figure 8 Raman spectra of strengite and variscite in the 900-1150  $\text{cm}^{-1}$  region.

The strengite Raman spectrum in the 900-1150  $\text{cm}^{-1}$  shows a strong band at 981  $\text{cm}^{-1}$  accompanied by a series of less intense bands (Fig. 8). The 981  $\text{cm}^{-1}$  band can be assigned to the phosphate symmetric stretching mode, while the weak band at 1116  $\text{cm}^{-1}$  is the corresponding antisymmetric stretching mode. The fact that this band is so weak is due to the orientation of the crystal lattice relative to the Raman laser beam. The remaining bands at 1009, 1023 and 1035  $\text{cm}^{-1}$  can be assigned to  $\nu_1(A_1)$  internal modes in analogy to the interpretation of the arsenate bands for scorodite and mansfieldite. It is a clear indication from the band splitting that the symmetry of the phosphate anion has been lowered from an ideal tetrahedron to a distorted tetrahedron.

The variscite Raman spectrum showed a shift towards higher wavenumbers in comparison to the strengite spectrum with the strongest band observed at 1030  $\text{cm}^{-1}$  (Fig. 8).



Similar bands were reported by Griffith [2] at  $1033\text{ cm}^{-1}$  and Frost, Weier, Erickson, Carmody and Mills [79] at  $1023\text{ cm}^{-1}$ , which shifted to  $1030\text{ cm}^{-1}$  at  $77\text{K}$ . This band can be assigned to the symmetric stretching vibration of the phosphate anion, while the corresponding antisymmetric stretching vibration can be observed at  $1080\text{ cm}^{-1}$ . Griffith [2] reported this band at  $1078\text{ cm}^{-1}$  and Frost, Weier, Erickson, Carmody and Mills [79] at  $1077\text{ cm}^{-1}$ . Due to the band splitting component bands were observed at  $1059$ ,  $1046$ ,  $1013$  and  $940\text{ cm}^{-1}$ . Similar bands were observed by e.g. Griffith [2] at  $1055\text{ cm}^{-1}$  and Frost, Weier, Erickson, Carmody and Mills [79] at  $1029$ ,  $1023$ ,  $1005$  and  $938\text{ cm}^{-1}$ . Based on the fact that the crystal structure of variscite accounts for only one type of phosphate tetrahedron and the fact that the extremely weak bands observed by Frost, Weier, Erickson, Carmody and Mills [79] between  $1150$  and  $1575\text{ cm}^{-1}$  are absent in this study, it is strange that they interpreted these multiple bands as an indication of multiple phosphate species in the variscite structure.

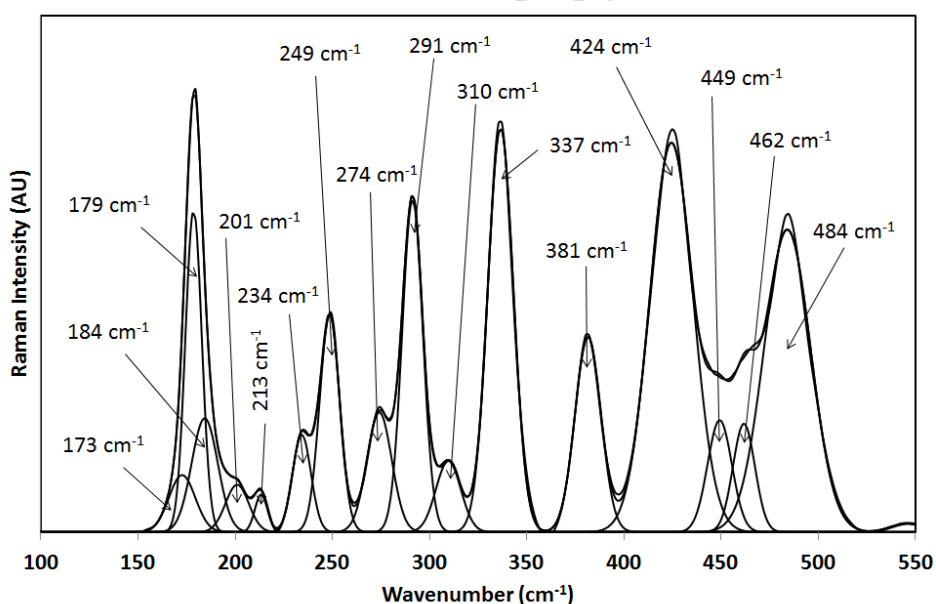


Fig. 8 Raman spectrum of scorodite in the  $100\text{-}550\text{ cm}^{-1}$  region.

In the wavenumber range below  $550\text{ cm}^{-1}$  a series of sharp bands can be observed (Fig. 9). Though Gomez, Assaoudi, Becze, Cutler and Demopoulos [59] reported only peak

positions and not detailed band fitting as in this study there is a good fit between the Raman spectra of their synthetic scorodite and the natural scorodite in this study (Table 3). The arsenate symmetric bending modes are observed at 381 and 337  $\text{cm}^{-1}$ , while corresponding antisymmetric bending modes occur at 424, 449 and 484  $\text{cm}^{-1}$ . It is unclear whether the band at 462  $\text{cm}^{-1}$  is an additional antisymmetric bending mode. The remaining bands are associated with lattice modes of Fe-O in the crystal structure of scorodite.

ACCEPTED MANUSCRIPT

Table 3 Raman bands for natural and synthetic scorodite (in  $\text{cm}^{-1}$ )

This study – natural scorodite	Gomez, Assaaoudi, Becze, Cutler and Demopoulos [59] – synthetic scorodite	Coleyshaw, Griffith and Bowell [60] – natural scorodite	Filippi, Machovic, Drahota and Bohmova [56]	Band assignment
			3600	OH stretch
3514	3516		3514	OH stretch
3082	3080		3427	OH stretch
			907	Antisymmetric stretch $\nu_3$ AsO <sub>4</sub>
890	880	889	893	Antisymmetric stretch $\nu_3$ AsO <sub>4</sub>
869	870		874	Antisymmetric stretch $\nu_3$ AsO <sub>4</sub>
830	830		831	Antisymmetric stretch $\nu_3$ AsO <sub>4</sub>
805	800	799	810	Symmetric stretch $\nu_1$ AsO <sub>4</sub>
786	-		799	OH deformation
			771	OH deformation
484	483		490	Antisymmetric bending $\nu_4$ AsO <sub>4</sub>
462				Antisymmetric bending $\nu_4$ AsO <sub>4</sub>
449	450		450	Antisymmetric bending $\nu_4$ AsO <sub>4</sub>
424	420	421	422	Antisymmetric bending $\nu_4$ AsO <sub>4</sub>
381	380	378	383	Symmetric bending $\nu_2$ AsO <sub>4</sub>
337	340	336	335	Symmetric bending $\nu_2$ AsO <sub>4</sub>
310	315			Lattice mode
291	292		293	Lattice mode
274	280		274	Lattice mode
249	250	243	251	Lattice mode
234	235			Lattice mode
213	215			Lattice mode
201	-			Lattice mode
184	-			Lattice mode
179	181		180	Lattice mode
173	-			Lattice mode
			135	Lattice mode

Raman spectroscopy is an excellent, fast and non-destructive technique for the study of and identification of a range of arsenate minerals. This can be applied not only to phase pure samples as used in the studies mentioned above, but also to identify the different minerals in e.g. polished sections. The knowledge of how the different arsenate vibrational

modes behave and the fingerprint of the lattice modes region make rapid identification possible.

## **Conclusions**

Scorodite, mansfieldite and variscite, as an environmentally important secondary arsenate minerals, were studied by Raman microscopy and X-ray Photoelectron Spectroscopy in order to gain a better understanding of this arsenate. The data obtained by this now relatively common non-destructive technique can be used to distinguish this mineral from other arsenates and related minerals in mine tailings and contaminated soils. Since a relatively large crystal in situ in the host rock was studied, the Raman spectrum and XPS spectra were clean and did not show anything associated with impurities. As a result a better understanding of the spectrum was achieved.

## **Acknowledgements**

The author wishes to thank the School of Chemistry, Physics and Mechanical Engineering, Science and Engineering Faculty, Queensland University of Technology for the use of their instrumentation. The authors acknowledge the facilities, and the scientific and technical assistance, of the Australian Microscopy & Microanalysis Research Facility at the Centre for Microscopy and Microanalysis, The University of Queensland.

## **References**

- [1] R.V. Gaines, H.C.W. Skinner, E.E. Foord, B. Mason, A. Rosenzweig, Dana's New Mineralogy - The System of Mineralogy of James Dwight Dana and Edward Salisbury Dana, Eighth Edition, John Wiley & Sons, Inc., New York, 1997.
- [2] W.P. Griffith, Raman studies on rock-forming minerals. II. Minerals containing MO<sub>3</sub>, MO<sub>4</sub>, and MO<sub>6</sub> groups, Journal of the Chemical Society [Section] A: Inorganic, Physical, Theoretical, (1970) 286-291.
- [3] A. Courtin-Nomade, H. Bril, J.-M. Beny, M. Kunz, N. Tamura, Sulfide oxidation observed using micro-Raman spectroscopy and micro-X-ray diffraction: the importance of water/rock ratios and pH conditions, Am. Mineral., 95 (2010) 582-591.
- [4] M. Filippi, Oxidation of the arsenic-rich concentrate at the Prebuz abandoned mine (Erzgebirge Mts., CZ): mineralogical evolution, Science of the Total Environment, 322 (2004) 271-282.
- [5] R.L. Flemming, K.A. Salzsauler, B.L. Sherriff, N.V. Sidenko, Identification of scorodite in fine-grained, high-sulfide, arsenopyrite mine-waste using micro X-ray diffraction ( $\mu$ XRD), Canadian Mineralogist, 43 (2005) 1243-1254.
- [6] M. Mihaljevic, V. Ettler, O. Sebek, P. Drahota, L. Strnad, R. Prochazka, J. Zeman, O. Sracek, Alteration of arsenopyrite in soils under different vegetation covers, Science of the Total Environment, 408 (2010) 1286-1294.
- [7] A. Murciego, E. Alvarez-Ayuso, E. Pellitero, M.A. Rodriguez, A. Garcia-Sanchez, A. Tamayo, J. Rubio, F. Rubio, J. Rubin, Study of arsenopyrite weathering products in mine wastes from abandoned tungsten and tin exploitations, Journal of Hazardous Materials, 186 (2011) 590-601.
- [8] P. Drahota, M. Filippi, Secondary arsenic minerals in the environment: a review, Environm. Int., 35 (2009) 1243-1255.

- [9] J.S. Ahn, Y.S. Park, J.-Y. Kim, K.-W. Kim, Mineralogical and geochemical characterization of arsenic in an abandoned mine tailings of Korea, *Environmental Geochemistry and Health*, 27 (2005) 147-157.
- [10] R.P. Borba, B.R. Figueiredo, J. Matschullat, Geochemical distribution of arsenic in waters, sediments and weathered gold mineralized rocks from Iron Quadrangle, Brazil, *Environmental Geology* (Berlin, Germany), 44 (2003) 39-52.
- [11] B.V. Brown, H.M. Valett, M.E. Schreiber, Arsenic transport in groundwater, surface water, and the hyporheic zone of mine-influenced stream-aquifer system, *Water Resources Research*, 43 (2007) W11404/11401-W11404/11414.
- [12] V.S.T. Ciminelli, F.L. Pantuzzo, Learning from the past: stability of arsenic in old mining residues, *Arsenic in Geosphere and Human Diseases, International Congress [on] Arsenic in the Environment*, 3rd, Tainan, Taiwan, May 17-21, 2010, (2010) 525-526.
- [13] D. Craw, P.O. Koons, D.A. Chappell, Arsenic distribution during formation and capping of an oxidised sulphidic minesoil, Macraes mine, New Zealand, *Journal of Geochemical Exploration*, 76 (2002) 13-29.
- [14] D. Craw, L. Pacheco, Mobilization and bioavailability of arsenic around mesothermal gold deposits in a semiarid environment, Otago, New Zealand, *TheScientificWorld* [online computer file], 2 (2002) 308-319.
- [15] S.L. DeSisto, H.E. Jamieson, M.B. Parsons, Influence of hardpan layers on arsenic mobility in historical gold mine tailings, *Applied Geochemistry*, 26 (2011) 2004-2018.
- [16] V. Ettler, Z. Johan, B. Kribek, O. Sebek, M. Mihaljevic, Mineralogy and environmental stability of slags from the Tsumeb smelter, Namibia, *Applied Geochemistry*, 24 (2009) 1-15.
- [17] V. Ettler, M. Mihaljevic, O. Sebek, Antimony and arsenic leaching from secondary lead smelter air-pollution-control residues, *Waste Management & Research*, 28 (2010) 587-595.

- [18] M. Filippi, B. Dousova, V. Machovic, Mineralogical speciation of arsenic in soils above the Mokrsko-west gold ore deposit, Czech Republic, *Geoderma*, 139 (2007) 154-170.
- [19] M. Filippi, V. Golias, Z. Pertold, Arsenic in contaminated soils and anthropogenic deposits at the Mokrsko, Roudny, and Kasperske Hory gold deposits, Bohemian Massif (CZ), *Environmental Geology* (Berlin, Germany), 45 (2004) 716-730.
- [20] F. Frau, C. Arda, Mineralogical controls on arsenic mobility in the Bacchu Locci stream catchment (Sardinia, Italy) affected by past mining, *Mineralogical Magazine*, 68 (2004) 15-30.
- [21] F. Frau, C. Arda, Geochemical controls on arsenic distribution in the Bacchu Locci stream catchment (Sardinia, Italy) affected by past mining, *Applied Geochemistry*, 18 (2003) 1373-1386.
- [22] L. Haffert, D. Craw, Geochemical processes influencing arsenic mobility at Bullendale historic gold mine, Otago, New Zealand, *New Zealand Journal of Geology and Geophysics*, 53 (2010) 129-142.
- [23] L. Haffert, D. Craw, Processes of attenuation of dissolved arsenic downstream from historic gold mine sites, New Zealand, *Science of the Total Environment*, 405 (2008) 286-300.
- [24] L. Haffert, D. Craw, Mineralogical controls on environmental mobility of arsenic from historic mine processing residues, New Zealand, *Applied Geochemistry*, 23 (2008) 1467-1483.
- [25] L. Haffert, D. Craw, J. Pope, Climatic and compositional controls on secondary arsenic mineral formation in high-arsenic mine wastes, South Island, New Zealand, *New Zealand Journal of Geology and Geophysics*, 53 (2010) 91-101.

- [26] E.J. Kim, J.-C. Yoo, K. Baek, Arsenic speciation and bioaccessibility in arsenic-contaminated soils: Sequential extraction and mineralogical investigation, *Environmental Pollution* (Oxford, United Kingdom), 186 (2014) 29-35.
- [27] E. Kocourkova, O. Sracek, S. Houzar, J. Cempirek, Z. Losos, J. Filip, P. Hrselova, Geochemical and mineralogical control on the mobility of arsenic in a waste rock pile at Dlouha Ves, Czech Republic, *Journal of Geochemical Exploration*, 110 (2011) 61-73.
- [28] J.H. Kyle, P.L. Breuer, K.G. Bunney, R. Pleyzier, Review of trace toxic elements (Pb, Cd, Hg, As, Sb, Bi, Se, Te) and their deportment in gold processing. Part II: Deportment in gold ore processing by cyanidation, *Hydrometallurgy*, 111-112 (2012) 10-21.
- [29] J. Mahoney, D. Langmuir, N. Gosselin, J. Rowson, Arsenic readily released to pore waters from buried mill tailings, *Applied Geochemistry*, 20 (2005) 947-959.
- [30] A. Parviainen, M.B.J. Lindsay, R. Perez-Lopez, B.D. Gibson, C.J. Ptacek, D.W. Blowes, K. Loukola-Ruskeeniemi, Arsenic attenuation in tailings at a former Cu-W-As mine, SW Finland, *Applied Geochemistry*, 27 (2012) 2289-2299.
- [31] L. Recio-Vazquez, J. Garcia-Guinea, P. Carral, A.M. Alvarez, F. Garrido, Arsenic Mining Waste in the Catchment Area of the Madrid Detrital Aquifer (Spain), *Water, Air, & Soil Pollution*, 214 (2011) 307-320.
- [32] K.A. Salzsauler, N.V. Sidenko, B.L. Sherriff, Arsenic mobility in alteration products of sulfide-rich, arsenopyrite-bearing mine wastes, Snow Lake, Manitoba, Canada, *Applied Geochemistry*, 20 (2005) 2303-2314.
- [33] M. Villalobos, D.G. Garcia-Payne, J.L. Lopez-Zepeda, A.E. Cenicerros-Gomez, M.E. Gutierrez-Ruiz, Natural Arsenic Attenuation via Metal Arsenate Precipitation in Soils Contaminated with Metallurgical Wastes: I. Wet Chemical and Thermodynamic Evidences, *Aquatic Geochemistry*, 16 (2010) 225-250.



- [34] S.R. Walker, M.B. Parsons, H.E. Jamieson, A. Lanzirrotti, Arsenic mineralogy of near-surface tailings and soils: influences on arsenic mobility and bioaccessibility in the Nova Scotia gold mining districts, *Canadian Mineralogist*, 47 (2009) 533-556.
- [35] N.V. Yurkevich, O.P. Saeva, N.A. Palchik, Arsenic mobility in two mine tailings drainage systems and its removal from solution by natural geochemical barriers, *Applied Geochemistry*, 27 (2012) 2260-2270.
- [36] E. Krause, V.A. Ettel, Solubility and stability of scorodite,  $\text{FeAsO}_4 \cdot 2\text{H}_2\text{O}$ : New data and further discussion, *Am. Mineral.*, 73 (1988) 850-854.
- [37] D. Langmuir, J. Mahoney, J. Rowson, Solubility products of amorphous ferric arsenate and crystalline scorodite ( $\text{FeAsO}_4 \cdot 2\text{H}_2\text{O}$ ) and their application to arsenic behavior in buried mine tailings, *Geochim. Cosmochim. Acta*, 70 (2006) 2942-2956.
- [38] A.J. Monhemius, P.M. Swash, Removing and stabilizing As from copper refining circuits by hydrothermal processing, *J. Metals*, 51 (1999) 30-33.
- [39] P. Gonzalez-Contreras, J. Weijma, C.J.N. Buisman, Continuous bioscorodite crystallization in CSTRs for arsenic removal and disposal, *Water Research*, 46 (2012) 5883-5892.
- [40] P. Gonzalez-Contreras, J. Weijma, R. van der Weijden, C.J.N. Buisman, Biogenic Scorodite Crystallization by *Acidianus sulfidivorans* for Arsenic Removal, *Environmental Science & Technology*, 44 (2010) 675-680.
- [41] N. Okibe, M. Koga, S. Morishita, M. Tanaka, S. Heguri, S. Asano, K. Sasaki, T. Hirajima, Microbial formation of crystalline scorodite for treatment of As(III)-bearing copper refinery process solution using *Acidianus brierleyi*, *Hydrometallurgy*, 143 (2014) 34-41.
- [42] R.J. Howell, J.V. Parshley, Control of pit-lake water chemistry by secondary minerals, Summer Camp pit, Getchell mine, Nevada, *Chemical Geology*, 215 (2005) 373-385.

- [43] A. Breithaupt, Skorodit, in: C.A.S. Hoffmann's Handbuch der Mineralogie, Verl. Craz & Gerlach, Freiberg, 1818, pp. 182-185.
- [44] F. Frau, A. Rossi, C. Ardaù, R. Biddau, S. Da Pelo, D. Atzei, C. Licheri, C. Cannas, G. Capitani, Determination of Arsenic Speciation in Complex Environmental Samples by the Combined Use of TEM and XPS, *Microchimica Acta*, 151 (2005) 189-201.
- [45] J.W. Anthony, R.A. Bideaux, K.W. Bladh, M.C. Nichols, *Handbook of Mineralogy Volume IV Arsenates, Phosphates, Vanadates*, Mineral Data Publishing, Tucson, Arizona, 2000.
- [46] V.T. Allen, J.J. Fahey, J.M. Axelrod, Mansfieldite, a new arsenate, the aluminum analogue of scorodite, and the mansfieldite-scorodite series, *Am. Mineral.*, 33 (1948) 122-132.
- [47] A. Breithaupt, Bestimmung neuer Mineralien 4. Variscit, *Journal für Praktische Chemie*, 10 (1837) 506-508.
- [48] J.W. Anthony, R.A. Bideaux, K.W. Bladh, M.C. Nichols, *Handbook of Mineralogy Volume IV - Arsenates, Phosphates and Vanadates*, Mineral Data Publishing, Tucson, Arizona, USA, 2000.
- [49] E.S. Larsen, E.V. Shannon, The minerals of the phosphate nodules from near Fairfield, Utah, *Am. Mineral.*, 15 (1930) 307-337.
- [50] A. Nies, Strengit, ein neues mineral, *Neues Jahrb. Mineral., Geol. Palaeont.*, (1877) 8-16.
- [51] J.G. Morales, R.R. Clemente, E. Matijevic, The mechanism of precipitation of colloidal variscite ( $\text{AlPO}_4 \cdot 2\text{H}_2\text{O}$ ) particles, *J. Coll. Interf. Sci.*, 151 (1992) 555-562.
- [52] R.W. McDowell, A.N. Sharpley, Phosphorus solubility and release kinetics as a function of soil test P concentration, *Geoderma*, 112 (2003) 143-154.

- [53] R.W. McDowell, N. Mahieu, P.C. Brookes, P.R. Poulton, Mechanisms of phosphorus solubilisation in a limed soil as a function of pH, *Chemosphere*, 51 (2003) 685-692.
- [54] S. Beauchemin, D. Hesterberg, J. Chou, M. Beauchemin, R.R. Simard, D.E. Sayers, Speciation of phosphorus in phosphorus-enriched agricultural soils using X-ray Absorption Near-Edge Structure Spectroscopy and chemical fractionation, *J. Environm. Qual.*, 32 (2003) 1809-1820.
- [55] P. Ondrus, R. Skala, C. Viti, F. Veselovsky, F. Novak, J. Jansa, Parascorodite,  $\text{FeAsO}_4 \cdot 2\text{H}_2\text{O}$  - a new mineral from Kank near Kutna Hora, Czech Republic, *Am. Mineral.*, 84 (1999) 1439-1444.
- [56] M. Filippi, V. Machovic, P. Drahota, V. Bohmova, Raman microspectroscopy as a valuable additional method to X-ray diffraction and electron microscope/microprobe analysis in the study of iron arsenates in environmental samples, *Applied Spectroscopy*, 63 (2009) 621-626.
- [57] S. Das, M.J. Hendry, Application of Raman spectroscopy to identify iron minerals commonly found in mine wastes, *Chemical Geology*, 290 (2011) 101-108.
- [58] Y. Jia, L. Xu, X. Wang, G.P. Demopoulos, Infrared spectroscopic and X-ray diffraction characterization of the nature of adsorbed arsenate on ferrihydrite, *Geochim. Cosmochim. Acta*, 71 (2007) 1643-1654.
- [59] M.A. Gomez, H. Assaaoudi, L. Becze, J.N. Cutler, G.P. Demopoulos, Vibrational spectroscopy study of hydrothermally produced scorodite ( $\text{FeAsO}_4 \cdot 2\text{H}_2\text{O}$ ), ferric arsenate sub-hydrate (FAsH;  $\text{FeAsO}_4 \cdot 0.75\text{H}_2\text{O}$ ) and basic ferric arsenate sulfate (BFAS;  $\text{Fe}[(\text{AsO}_4)_{1-x}(\text{SO}_4)_x(\text{OH})_x] \cdot w\text{H}_2\text{O}$ ), *Journal of Raman Spectroscopy*, 41 (2010) 212-221.
- [60] E.E. Coleyshaw, W.P. Griffith, R.J. Bowell, Fourier-transform Raman spectroscopy of minerals, *Spectrochimica Acta, Part A: Molecular and Biomolecular Spectroscopy*, 50A (1994) 1909-1918.

- [61] K. Kitahama, R. Kiriyaama, Y. Baba, Refinement of the crystal structure of scorodite, *Acta Crystallographica, Section B: Structural Crystallography and Crystal Chemistry*, B31 (1975) 322-324.
- [62] D.R. Baghurst, J. Barrett, E.E. Coleyshaw, W.P. Griffith, D.M.P. Mingos, Microwave techniques for the synthesis and deuteration of minerals, with particular reference to scorodite, *FeAsO<sub>4</sub>·H<sub>2</sub>O*, *Mineralogical Magazine*, 60 (1996) 821-828.
- [63] F.C. Hawthorne, The hydrogen positions in scorodite, *Acta Crystallographica, Section B: Structural Crystallography and Crystal Chemistry*, B32 (1976) 2891-2892.
- [64] S.C.B. Myneni, S.J. Traina, G.A. Waychunas, T.J. Logan, Experimental and theoretical vibrational spectroscopic evaluation of arsenate coordination in aqueous solutions, solids, and at mineral-water interfaces, *Geochim. Cosmochim. Acta*, 62 (1998) 3285-3300.
- [65] M.A. Gomez, L. Becze, M. Celikin, G.P. Demopoulos, The effect of copper on the precipitation of scorodite (*FeAsO<sub>4</sub>·2H<sub>2</sub>O*) under hydrothermal conditions: Evidence for a hydrated copper containing ferric arsenate sulfate-short lived intermediate, *Journal of Colloid and Interface Science*, 360 (2011) 508-518.
- [66] R.L. Frost, J.T. Kloprogge, W.N. Martens, Raman spectroscopy of the arsenates and sulphates of the tsumcorite mineral group, *Journal of Raman Spectroscopy*, 35 (2004) 28-35.
- [67] R.L. Frost, W.N. Martens, P.A. Williams, J.T. Kloprogge, Raman spectroscopic study of the vivianite arsenate minerals, *Journal of Raman Spectroscopy*, 34 (2003) 751-759.
- [68] J.T. Kloprogge, R.L. Frost, Raman microscopy study of cafarsite, *Applied Spectroscopy*, 53 (1999) 874-880.
- [69] W.N. Martens, R.L. Frost, J.T. Kloprogge, Raman spectroscopy of synthetic erythrite, partially dehydrated erythrite and hydrothermally synthesized dehydrated erythrite, *Journal of Raman Spectroscopy*, 34 (2003) 90-95.

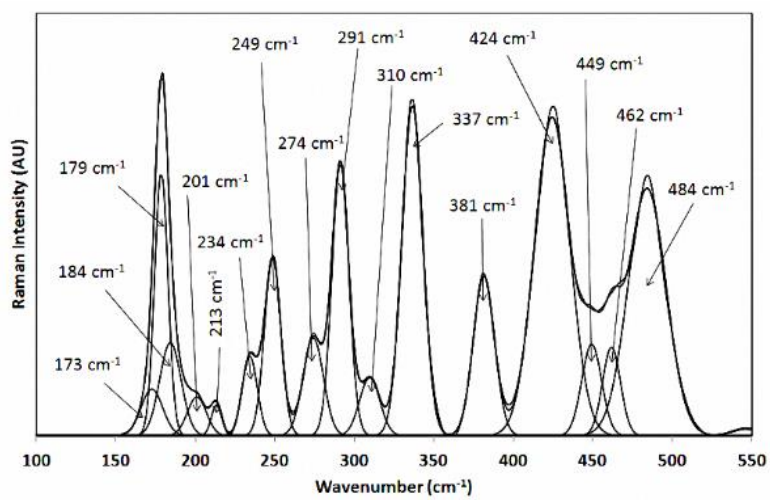
- [70] W.N. Martens, R.L. Frost, J.T. Kloprogge, P.A. Williams, The basic copper arsenate minerals olivenite, cornubite, cornwallite, and clinoclase: an infrared emission and Raman spectroscopic study, *Am. Mineral.*, 88 (2003) 501-508.
- [71] W.N. Martens, J.T. Kloprogge, R.L. Frost, L. Rintoul, Site occupancy of Co and Ni in erythrite-annabergite solid solutions deduced by vibrational spectroscopy, *Canadian Mineralogist*, 43 (2005) 1065-1075.
- [72] W.N. Martens, J.T. Kloprogge, R.L. Frost, L. Rintoul, Single-crystal Raman study of erythrite,  $\text{Co}_3(\text{AsO}_4)_2 \cdot 8\text{H}_2\text{O}$ , *Journal of Raman Spectroscopy*, 35 (2004) 208-216.
- [73] M. Wojdyr, Fityk: a general-purpose peak fitting program, *J. Appl. Cryst.*, 43 (2010) 1126-1128.
- [74] J.T. Kloprogge, L.V. Duong, B.J. Wood, R.L. Frost, XPS study of the major minerals in bauxite: Gibbsite, bayerite and (pseudo-)boehmite, *Journal of Colloid and Interface Science*, 296 (2006) 572-576.
- [75] E. Görlich, J. Haber, A. Stoch, J. Stoch, XPS study of  $\alpha$ -quartz surface, *J. Solid State Chem.*, 33 (1980) 121-124.
- [76] M. Jakubith, G. Lehmann, An X-ray photoelectron spectroscopic study of shock-loaded quartz, *Phys. Chem. Minerals*, 7 (1981) 165-168.
- [77] M.A. Gomez, J.-F. Le Berre, H. Assaoudi, G.P. Demopoulos, Raman spectroscopic study of the hydrogen and arsenate bonding environment in isostructural synthetic arsenates of the variscite group -  $\text{M}^{3+}\text{AsO}_4 \cdot 2\text{H}_2\text{O}$  ( $\text{M}^{3+} = \text{Fe}, \text{Al}, \text{In}$  and  $\text{Ga}$ ): implications for arsenic release in water, *Journal of Raman Spectroscopy*, 42 (2011) 62-71.
- [78] S.D. Ross, Phosphates and other oxy-anions of group V, in: V.C. Farmer (Ed.) *The Infrared Spectra of Minerals*, Mineralogical Society, London, 1974.

[79] R.L. Frost, M.L. Weier, K.L. Erickson, O. Carmody, S.J. Mills, Raman spectroscopy of phosphates of the variscite mineral group, *Journal of Raman Spectroscopy*, 35 (2001) 1047-1055.

[80] K.S. Savage, D.K. Bird, P.A. O'Day, Arsenic speciation in synthetic jarosite, *Chemical Geology*, 215 (2005) 473-498.

ACCEPTED MANUSCRIPT

## Graphical Abstract



## Highlights

- Variscite, strengite, mansfieldite and scorodite play important role in mine waste
- XPS and Raman Spectroscopy are non-destructive, quick methods to identify minerals
- XPS data were obtained of single crystals in situ in a vug in original host rock
- XPS showed the compositions of variscite, strengite, mansfieldite and scorodite
- Raman spectra of the same crystals were interpreted regarding the OH, AsO<sub>4</sub> and PO<sub>4</sub>

ACCEPTED MANUSCRIPT